IEEE Access
Multidisciplinary | Rapid Review | Open Access Journal

Received April 25, 2018, accepted May 30, 2018, date of current version July 6, 2018.

Digital Object Identifier 10.1109/ACCESS.2018.2846585

Continuous Wavelet Transform Based No-Reference Image Quality Assessment for Blur and Noise Distortions

PIYUSH JOSHI AND SURYA PRAKASH
Department of CSE, IIT Indore, Indore 452020, India

Corresponding author: Piyush Joshi (phd1301101004@iiti.ac.in)

This work was supported by the Science and Engineering Research Board, Department of Science and Technology, Government of India, under Grant SB/FTP/ETA-0074/2014.

ABSTRACT This paper proposes a no-reference quality assessment technique to assess the quality of images that is degraded due to blur and noise. The technique is motivated from the fact that when distortion occurs in a natural image, its naturalness gets disturbed. We analyze this disturbance using continuous-wavelet transform in order to assess the quality of the image. The proposed image quality estimation technique is free from training and prior knowledge of the distortion (noise or blur) present in the image. The technique is being evaluated on LIVE and CSIQ databases, and the obtained results are found very similar with subjective scores provided by the databases. It is observed from the obtained results that the proposed technique outperforms the latest state-of-the-art techniques.

INDEX TERMS Image quality assessment, no-reference image quality assessment, continuous wavelet transform.

I. INTRODUCTION

Multimedia network technology has enabled us to share information through digital images conveniently. While handling of the images, there are chances of images getting distorted at several stages such as image acquisition, compression, transmission, processing, and reconstruction. Further, it becomes very difficult to extract information from distorted images for understanding and subsequent analysis. Therefore, identifying and quantifying the distortions are very important to control and enhance the distorted images. This inspires us to propose an image quality assessment (IQA) technique. Image quality can be defined as a measure to quantitatively estimate the perceptual quality of an image. The practical importance of IQA techniques has been discussed in [1] and [2] in detail. IQA techniques are divided into three types: no-reference (NR), reduced-reference (RR) and full reference (FR) [3]. In FR-IQA, the quality of an image is computed by comparing it with a reference image (the original version of the distorted image). In RR-IQA, partial information of the reference image is used to estimate the quality of a distorted image. In NR-IQA, there is no need of any reference image to estimate quality of a distorted image. In most of the practical scenarios, reference image (original image) for the distorted image is not present and hence NR-IQA is the exclusive practical approach for quality estimation.

The rest of the paper is structured as follows. Section II presents literature survey on NR-IQA techniques. Section III shows required preliminaries. The proposed technique is presented in Section IV. Experimental results are discussed in Section V. Finally, paper is concluded in Section VI.

II. LITERATURE SURVEY

NR-IQA techniques are divided into two types: first, quality assessment techniques for specific distortion and second, quality assessment techniques for general purpose. Distortion specific quality assessment techniques estimate quality using foreknowledge of the distortion. JP2K distortion based quality is estimated using edge information and pixel distortions in [4]. JPEG (blocking artifacts) distortion has been assessed in [5] which used the power of the blocky signal to estimate the image quality. Blocking artifacts has been estimated using Discrete Cosine Transform (DCT) in the technique proposed in [6]. In another technique proposed in [7], blocking artifacts are measured using block-edge impairment metric. A machine learning technique to measure blocking artifacts is proposed in [8]. Color changing properties, block boundary and image corner have

been utilized in this technique to estimate image quality. A full and NR blur metric as well as a full reference ringing metric are utilized in technique proposed in the [9] to estimate image quality. This technique has extracted features based on adjacent regions and edges in an image. Blocking and ringing artifacts (JPEG2000) are estimated in technique proposed in [10]. This technique has utilized histogram computed using sharpness distribution of the gradient profiles to estimate blur and has utilized visibilities regions of gradient profiles to estimate ringing artifacts. Blur and ringing based quality are combined to get final quality score. Blur based quality is estimated using Edge spreading [11]. A blind IQA technique is presented in [12] which has utilized discrete Tchebichef moments to estimate blur distortion. Blur distortion has been estimated in [13] which has used natural scenes statistics (NSS) model and this model is combined with multi-resolution decomposition techniques to estimate quality of the image. A no-reference technique called robust image sharpness evaluation (RISE) is proposed in [14] which has utilized learning using multiscale features of spatial and spectral domains to estimate image quality. A no-reference technique proposed in [15] has utilized CWT to assess quality of deblocked images. All above mentioned techniques are proposed to measure only single distortion. Moreover, most of them rely on training to estimate image quality.

General purpose quality assessment techniques estimate image quality by considering multiple distortions. Distorted image statistics (DIS) feature has been utilized in [16] for classifying distortions using support vector machine (SVM) and further, probability obtained by the SVM is used to compute amount of distortion. NSS features in DCT domain are used in the technique called BLIINDS presented in [17] to assess image quality. NSS based features in wavelet domain are utilized in technique DIIVINE proposed in [18]. This technique has identified distortion using scene statistics features extracted from the image. Further, these statistics are utilized to estimate the distortion-specific image quality. The technique proposed in [19] has used NSS features in curvelet domain to estimate the image quality. This IQA technique has utilized log-histograms and energy distributions of curvelet coefficients for quality estimation. BRISQUE technique proposed in [20] has estimated image quality using NSS features in spatial domain. Few significant statistics such as distortion texture, complex wavelet domain and blur/noise statistics are utilized in [21] to make features for training in order to assess quality of the image. The technique presented in [22] has used Gabor wavelet features of patches of original images to compute visual codebooks and then estimate the image quality using support vector machine (SVM).

All the above techniques are general purpose IQA techniques, however, they heavily depend on training using human scores of distorted images and hence their scope is highly relied on distortions provided for training.

Recently, there are a few IQA techniques available in the literature which depend on training without human scores of distorted images. A technique proposed in [23] named Quality-Aware Clustering (QAC) has utilized original images and their distorted images for training to estimate image quality. NSS features based training (without human scores) has utilized in [24] to estimate the image quality. Another IQA technique proposed in [25] has used mean gradient magnitude, mean phase congruency and entropy to estimate quality of an image. A technique proposed in [26] computes Multivariate Gaussian Model (MVG) using NSS based features of original images to assess quality of images. All the techniques discussed in this paragraph use training based on distorted and/or pristine images.

A recent work on NR-IQA for multiple distortions is presented in [27] which does not use any training. Another training free IQA technique is presented in [28] which has utilized information of structural activity of multiple visual significance present in the image. In our previous work in [29], we have presented no-reference, no-training based IQA technique to estimate quality of images distorted by noise and blur. This technique has generated multiple DoG images using multiple frequencies. Further, edge and entropy features are extracted from DoG images to assess quality of the image.

In this work, we propose an efficient no-reference no-training based IQA technique to estimate quality of images distorted due to blur and noise. The proposed technique relies on the fact that presence of distortions disturbs the naturalness of an image and uses it to assess quality of the image. We have utilized CWT with Mexican hat as a mother wavelet to estimate the image quality. The proposed technique does not need any reference image as well as is free from any training to assess the quality of an image. It performs superior to existing no-reference no-training based IQA techniques in the literature.

III. PRELIMINARIES

This section presents a few preliminaries for the proposed technique. These preliminaries include understanding the properties of a natural image and CWT.

A. UNDERSTANDING THE PROPERTIES OF A NATURAL IMAGE

According to Retinex [30] model, natural image can be decomposed into two components, *viz*. illumination and reflectance. Out of these two components, illumination represents low frequency whereas reflectance depicts high frequency information. A balance must be maintained between these two information to have a good quality image [31]. The extremely low frequency may flood details (blur image) whereas the extremely high frequency may result into unnaturalness (noisy image). Human being observe both high and low frequencies in every part of the image [30]. The significant point to be noted is the *"every part"* which defines local information in an image. To elaborate on this notion, let us consider an example depicted in Figure 1 where Figure 1(a) shows a natural image and Figure 1(b) shows a noisy image. Image in Figure 1(a) globally contains more high frequency

(a) Natural image (b) Noisy image

FIGURE 1. Image (a) depicts a natural image (noise-free) and image (b) shows a noisy image with $\sigma = 0.062$.

than the noisy image of Figure 1(b). However, a human perceives that the image in Figure 1(a) is noise free whereas image in Figure 1(b) contains noise. This happens due to the fact that the image in Figure 1(a) contains both high and low both frequencies in different parts of the image whereas the image in Figure 1(b) has mostly high frequency in most parts of the image. Inspired by this Human Visual System (HVS) phenomenon, we compute block by block naturalness of the image using CWT to estimate the quality of an image.

B. CONTINUOUS WAVELET TRANSFORM (CWT)

CWT [32] is used to divide a continuous-time function into wavelets. CWT computes inner products between an analyzing function and a signal to measure the similarity. CWT of function $f(t)$ is given as:

$$C(a, b, f(t), \psi) = \int_{-\infty}^{\infty} f(t) \frac{1}{\sqrt{a}} \psi^*(\frac{t-b}{a}) dt$$

where, a is scale parameter, b represents position, ψ is the analyzing function (called mother wavelet) and $*$ denotes the complex conjugate. The proposed technique uses Mexican hat function as mother wavelet. Mexican hat function is the second derivative of a Gaussian function. The reason behind choosing the Mexican hat wavelet as mother wavelet in our study is due to the fact that it consists of important traits such as smoothness (regularity), symmetry, and a very rapid decay. All these traits are similar to those of the human eye [33].

IV. PROPOSED TECHNIQUE

It is observed that a natural image contains certain statistical properties which if get disturbed due to distortions, degrade the quality of an image. The proposed technique exploits these properties of a natural image to estimate its quality. It evaluates these disturbances with the help of histogram of CWT coefficients and use them in quality estimation. Figure 2 provides overall framework of the proposed technique. The technique first divides input image into blocks and then computes CWT of each block. Further for each block, histogram of CWT coefficients is computed and features from the histogram are extracted. These features are subsequently utilized in quality estimation of the image.

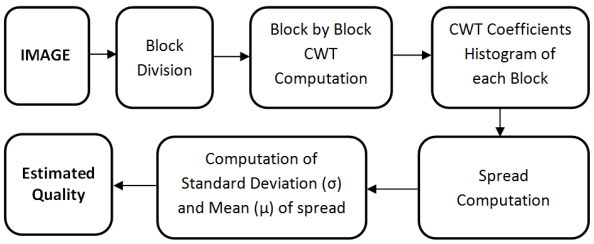

FIGURE 2. Framework of the proposed technique.

A. HISTOGRAM OF CWT COEFFICIENTS

Histogram of CWT coefficients plays significant role in the proposed technique in estimation of quality of an image. Following discussion provides steps involved in the histogram computation.

1) First of all, input image I is broken into blocks of size $m \times m$.
2) CWT is computed for each block using low scale (*i.e.*, *scale* $=$ 1, low scale indicates higher frequency) of Mexican hat mother wavelet. CWT coefficients obtained using low scale of Mexican hat mother wavelet are large in presence of high frequency in signal whereas they found small otherwise [15].
3) CWT coefficients image (of size $m \times m$) obtained for each block in the previous step is normalized in the range of -128 to 127 where each value represents the magnitude of the coefficient. We have used this range for normalization to get 256 bins in the histogram.
4) Finally, histogram of each coefficient image obtained in the previous step is computed considering 256 number of bins.

B. FEATURE EXTRACTION FROM CWT COEFFICIENT HISTOGRAM

Our hypothesis is that the histogram of CWT coefficients of a natural image contains certain properties and these properties get affected in presence of distortions. This phenomenon can be visualized from Figures 3 and 4 which show histogram of CWT coefficients of three distinct blocks of different types of images *viz.* blurred, natural and noisy images.

In a blurred image (which contains mostly low frequencies), mother wavelet (with *scale* $=$ 1 and representing high frequency) is found to be less similar to the signal and hence low value coefficients (poor matching) are obtained while wavelet decomposition. All these coefficients create a peak on lower side (near zero) of the histogram and make a bell shape structure. Also, it is observed that height of the peak increases as the blur increases.

On the other hand, in a noisy image (which mostly contains high frequencies), mother wavelet (which represents low scale and high frequency) matches well with the high frequencies and due to this, few low and more number of high value coefficients are obtained while wavelet decomposition. As a result, obtained histogram looks flat and almost equally distributed all over the range. A natural image is a middle case

of blur and noise and contains almost a balanced mixture of high and low frequencies, and hence the amount of peakiness in the histogram of CWT coefficient image of a natural image is found to be in between the same obtained for a blurred and a noisy images. This phenomenon is explained below with the help of few examples.

Histograms of blurred images are analyzed in Figure 3 where Figure 3(a) shows a natural image and Figure 3(b) shows histograms of CWT images of its three blocks marked by red squares in the image. Blurred images generated from this natural image (Figure 3(a)) are shown in Figures 3(c), (e) and (g), where amount of blur increases as we move from top to bottom, *i.e.* image in Figure 3(c) has the lowest level of blur whereas the image in Figure 3(g) has the highest level of blur. From the histograms shown in Figures 3(d), (f) and (h) corresponding to the images shown in Figures 3(c), (e) and (g), it can be seen that as the level of blur in the image increases, more and more low value CWT coefficients are obtained and as a result histogram of CWT coefficients (as we see in all three histograms of different blocks in blurred images) shrinks towards making a sharp peak near zero.

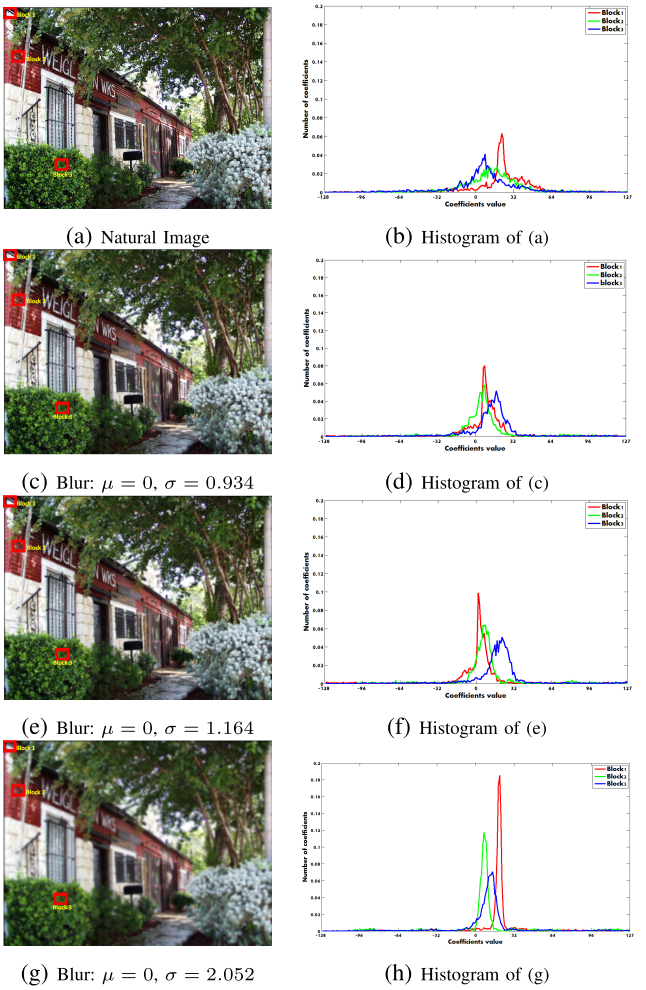

(a) Natural Image (b) Histogram of (a)
(c) Blur: $\mu = 0$, $\sigma = 0.934$ (d) Histogram of (c)
(e) Blur: $\mu = 0$, $\sigma = 1.164$ (f) Histogram of (e)
(g) Blur: $\mu = 0$, $\sigma = 2.052$ (h) Histogram of (g)

FIGURE 3. Examples of histograms of three blocks (marked by red squares) of few blurred images: (a) is natural image and (b) is its histogram. Blurred images with their respective mean (μ) and standard deviation (σ) are shown in (c), (e) and (g), and their respective histograms are shown in (d), (f) and (h).

Histograms of noisy images are analyzed in Figure 4. Figures 4(c), (e) and (g) show noisy images where level of noise increases as we move from top to bottom, *i.e.* image in Figure 4(c) has the lowest level of noise whereas image in Figure 4(g) has the highest level of noise. From the histograms shown in Figures 4(d), (f) and (h) corresponding to the images shown in Figures 4(c), (e) and (g), it can be seen that as level of noise in the image increases, more and more high value CWT coefficients are obtained and as a result histogram of CWT coefficients (as we see in all three histograms of different blocks in noisy images) becomes more and more distributed over the range.

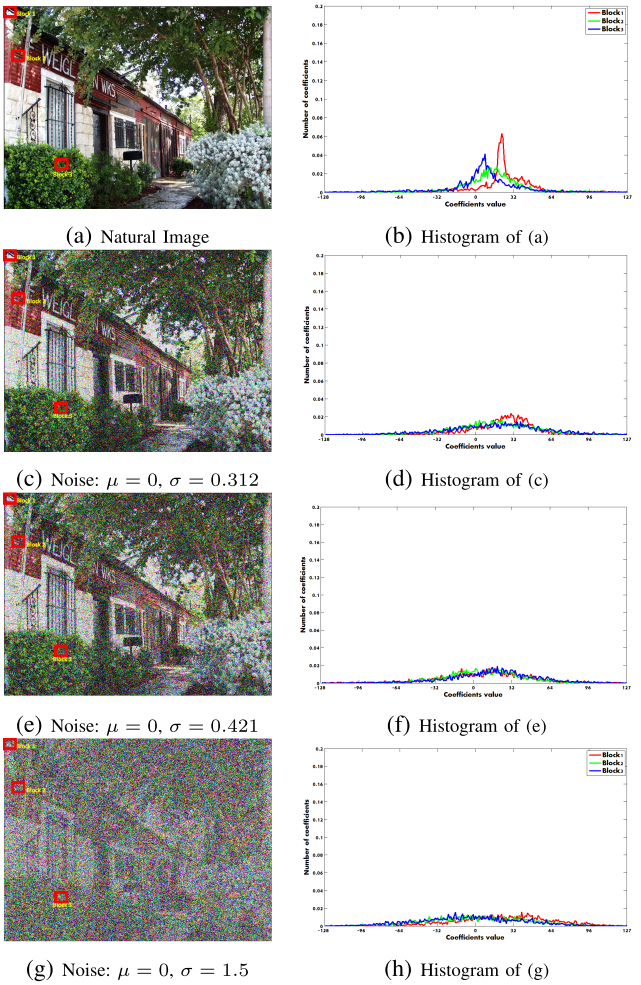

(a) Natural Image (b) Histogram of (a)
(c) Noise: $\mu = 0$, $\sigma = 0.312$ (d) Histogram of (c)
(e) Noise: $\mu = 0$, $\sigma = 0.421$ (f) Histogram of (e)
(g) Noise: $\mu = 0$, $\sigma = 1.5$ (h) Histogram of (g)

FIGURE 4. Examples of histograms of three blocks (marked by red squares) of few noisy images: (a) is natural image and (b) is its histogram. Noisy images with their respective mean (μ) and standard deviation (σ) are shown in (c), (e) and (g), and their respective histograms are shown in (d), (f) and (h).

It is to note that the number of high frequency CWT coefficients present in an image is inversely proportional to the amount of blur present in the image.

On contrary, in case of noise, the number of high frequency CWT coefficients are found to be proportional to the amount of noise present in the image. This means that the count of high frequency CWT coefficients increases as noise in the image increases whereas, it decreases when blur in the image increases. In both these extreme cases (*i.e.* when more number of large value high frequency CWT coefficients exist due to high noise or when very less number of large value high frequency CWT coefficients exist due to high blur), quality of the image is low. For a good quality image, value of high frequency CWT coefficients is expected to be approximately at the middle of these two extreme situations.

We propose to distinguish blurred, natural and noisy images and compute their quality based on the patterns of their CWT histograms. We use the notion of spread of a histogram for this purpose. Spread of a histogram defines how wide is its distribution from the peak. It is calculated by counting the number of coefficients of the bins in the histogram which are α distant from the peak. Formally, spread is defined as follows.

$$spread = \int_{q_l}^{q_u} h(q)dq \tag{1}$$

where, $h(q)$ represents the value of the q^{th} bin in the histogram and $q \in [1, 256]$. Further, q_l and q_u are the intersection points of histogram h and threshold line $l(q) = (1 - \alpha) * h_{max}$ where h_{max} represents the value of max bin (peak) in the histogram. Here, $\alpha \in [0, 1]$ and is used to obtain bins (whose bin values are α distant from the peak) which participate in spread computation.

Figure 5 pictorially presents the process of spread computation. We compute the spread of a histogram considering a set of values of α and take the average to get final spread value. We adopt this to make the assessment more robust and capable of effectively handling the variability in the histograms of different kinds of images.

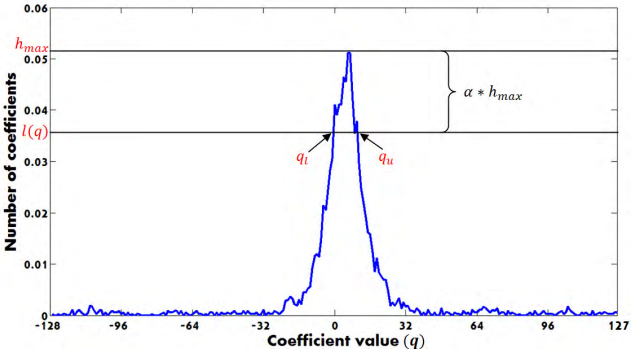

FIGURE 5. Pictorial representation of spread computation.

Figure 6 shows the spread values computed for blurred, natural and noisy images where the image is broken into non-overlapping blocks of size 50 × 50 and spread values are computed for histogram of each block. As expected, in case of a blurred image, spread values are found to be low since

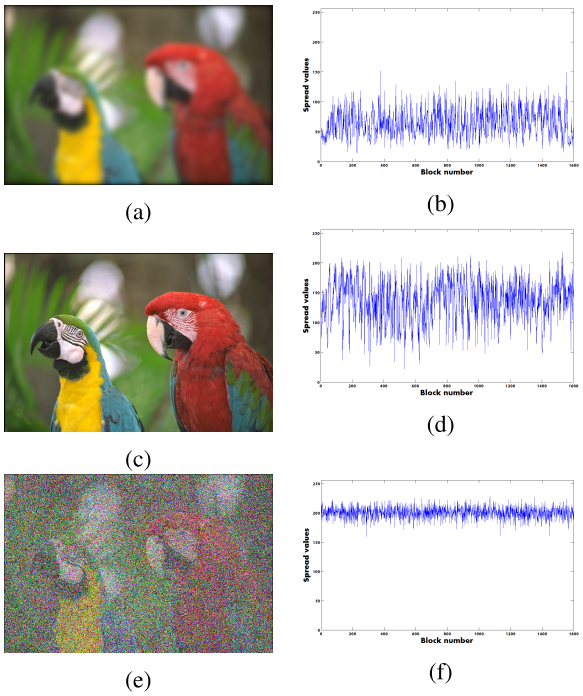

FIGURE 6. Histograms of spread values computed for different blocks of blurred, natural and noisy images. (a) Gaussian blur: $\mu = 0$, $\sigma = 3.54$. (b) Spread for blurred image. (c) Natural image. (d) Spread for natural image. (e) white noise: $\mu = 0$, $\sigma = 1.0$. (f) Spread for noisy image.

blocks contain low frequencies and hence a peaky histogram is obtained for CWT coefficient images. Figure 6(b) shows spread values computed for various blocks of a blurred image shown in Figure 6(a). In case of a noisy image, histogram of CWT coefficients is distributed and hence leads to high spread values. Figure 6(f) shows spread values of various blocks of a noisy image shown in Figure 6(e). Since a natural image contains almost a balanced mixture of low and high frequencies, we observe spread values in this case not as much as in case of noisy images and not as less as in case of blurred images. This can be seen from the Figure 6(d) which shows spread values computed from different blocks of the natural image shown in Figure 6(c).

C. QUALITY ASSESSMENT

Quality assessment of an image is carried out using the spread information of the histograms. We utilize the values of mean (μ_s) and standard deviation (σ_s) of the spread to compute the quality. It can be noted that as we compute histogram of CWT coefficients using 256 bins, the value of spread obtained from Equation 1 would lie in the range of 0 to 256, *i.e.* the minimum and the maximum values obtained for *spread* would be 0 and 256 respectively. Hence, if we analyze the mean (μ_s) value of spread for all the blocks of an image, it would vary in the range of 0 to 256. Similarly, it can be visualized that the value of standard deviation (σ_s) of spread for all the blocks of an image would range from 0 to 128.

Figures 7 and 8 demonstrate how mean (μ_s) and standard deviation (σ_s) vary with respect to variations in noise and

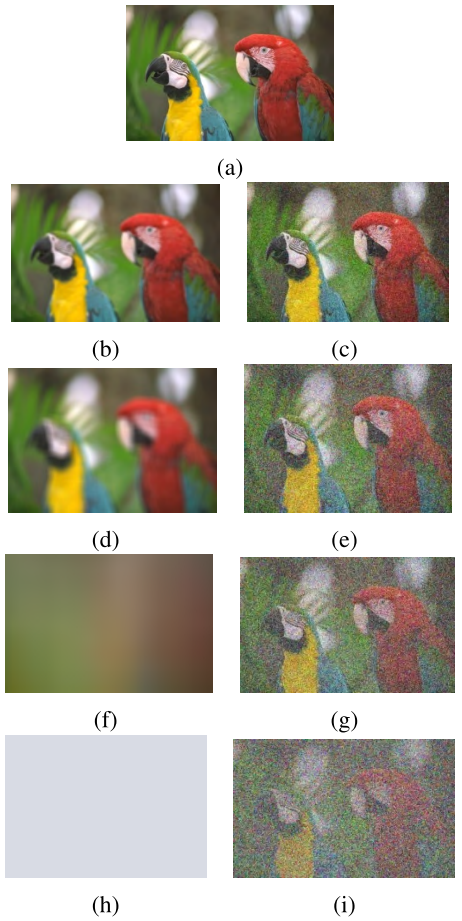

FIGURE 7. Example of images with different amount of blur and noise: I_1: original image, from image I_2 to image I_5: increasing level of blur, from image I_6 to image I_9: increasing level of noise. (a) I_1. (b) I_2. (c) I_6. (d) I_3. (e) I_7. (f) I_4. (g) I_8. (h) I_5. (i) I_9.

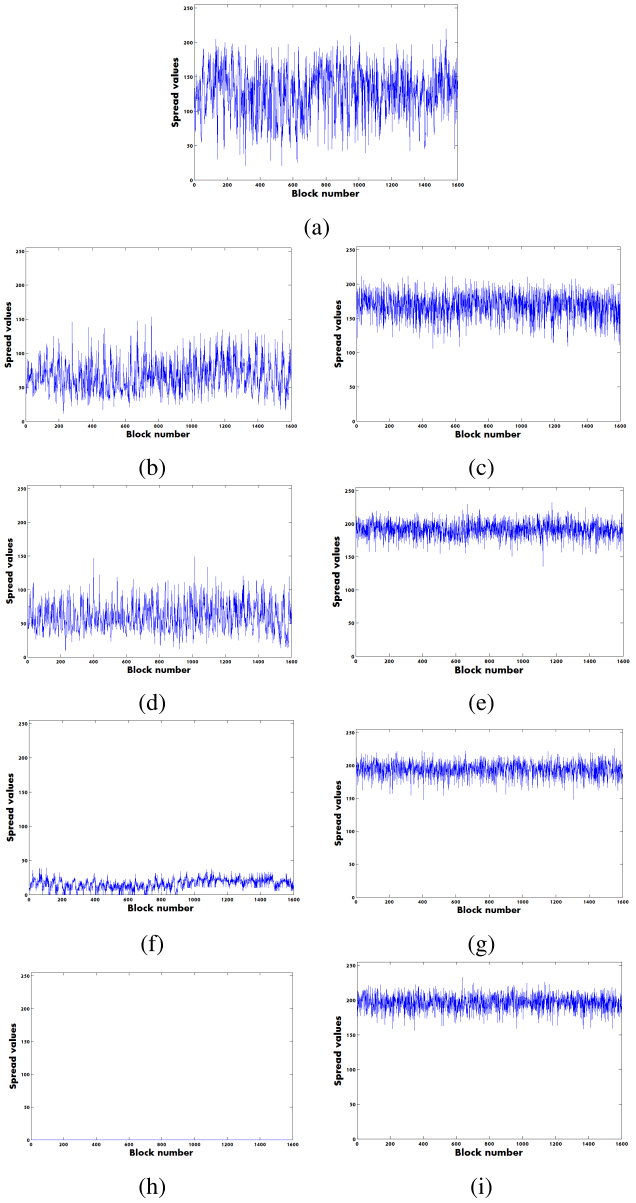

FIGURE 8. Demonstration of change in mean (μ_s) and standard deviation (σ_s) of spread with respect to variations in blur and noise. Corresponding spread plots of the images shown in Figure 7 (X-axis: Block number, Y-axis: Spread values). (a) $I_1 : \mu_s = 119, \sigma_s = 54$. (b) $I_2 : \mu_s = 88, \sigma_s = 48$. (c) $I_6 : \mu_s = 176, \sigma_s = 27$. (d) $I_3 : \mu_s = 50, \sigma_s = 30$. (e) $I_7 : \mu_s = 196, \sigma_s = 20$. (f) $I_4 : \mu_s = 10, \sigma_s = 18$. (g) $I_8 : \mu_s = 210, \sigma_s = 14$. (h) $I_5 : \mu_s = 0, \sigma_s = 0$. (i) $I_9 : \mu_s = 215, \sigma_s = 10$.

blur, where Figure 8 shows spread plots for the images shown in Figure 7. In Figure 7, image I_1 is the original image and its computed μ_s and σ_s values of spread are 119 and 54 respectively. Further it can be observed from images I_2 to I_5 that as the blur increases, the values of both μ_s and σ_s decrease. It can be noticed that the extreme blurred image I_5 (obtained synthetically) has $\mu_s = 0$ and $\sigma_s = 0$. Further, it can be observed from images I_6 to I_9 that as the noise increases, the value of μ_s increases whereas the value of σ_s decreases. The extreme noisy image I_9 has $\mu_s = 215$ and $\sigma_s = 10$. To summarize, the value of μ_s varies in the range of 0 to 256 where 0 depicts extreme blur while 256 depicts the extreme noisy case and the value of σ_s varies in the range of 0 to 128 where both the extreme cases of noise and blur have σ_s equal to 0.

It is observed that as blur in an image increases, its histogram of CWT coefficients becomes more and more peaky and as a result spread of the histogram tends to decrease. Hence mean of the spread of histograms computed for all the blocks also tends to decrease as blur increases. Similarly, histogram of the CWT coefficients of the image becomes more and more distributed when noise in the image increases. This in turn indicates the increase in the spread of the histograms of all the blocks of the image. Due to this, mean of the spread of histograms computed for all the blocks in a noisy image tends to increase as noise level increases. Since a histogram of CWT coefficients is computed using 256 bins, we observe that as an image undergoes changes from extreme blur to extreme noise, the mean value of spread changes from 0 to 256. Since a good image should lie in between the cases of extreme blur and extreme noise, we assume that the middle value of mean of the spread (*i.e.* 128) expresses the best quality. Standard deviation of spread represents variability in

the image and it should not be very high (standard deviation near 128) or very low (standard deviation near 0) for a good quality image. Therefore we consider middle value of the standard deviation, which is 64, to represent the best quality image.

Based on the obtained values of mean (μ_s) and standard deviation (σ_s) of the spread, the proposed technique computes quality Q of an image as follows:

case a)

1) If $\mu_s \leq 128$

$$Q = \begin{cases} \frac{\mu_s}{128} \times \frac{\sigma_s}{64}, & \text{if } \sigma_s \leq 64 \\ \frac{\mu_s}{128} \times \frac{128 - \sigma_s}{64}, & \text{otherwise} \end{cases} \quad (2a)$$

2) If $\mu_s > 128$

$$Q = \begin{cases} \frac{\sigma_s}{64} \times \frac{128}{\mu_s}, & \text{if } \sigma_s \leq 64 \\ \frac{128 - \sigma_s}{64} \times \frac{128}{\mu_s}, & \text{otherwise} \end{cases} \quad (2b)$$

The proposed technique defines quality of an image in the range of 0 and 1 where 0 shows the worst quality whereas 1 shows the best quality. Based on the above equations (2a and 2b), we can devise following four cases.

1) **Case 1**: When both mean (μ_s) and standard deviation (σ_s) of the spread are 0, it represents the presence of extreme blur in the image and the image quality Q is obtained as 0.
2) **Case 2**: When μ_s and σ_s are 256 and 0 respectively, it represents the presence of extreme noise in image, and the obtained image quality Q is 0.
3) **Case 3**: When σ_s is high (close to 128), *i.e.* presence of extreme fluctuation in the spread plot, it is again an indication of poor image quality (*i.e.* image quality Q equals to 0). Example of one such case is shown in Figure 9 where Figure 9(a) shows an image with half blurred and half noisy, a case of poor quality image. The spread plot for this image (presented in Figure 9(b)) shows quite high standard deviation ($\sigma_s = 101$).
4) **Case 4**: When μ_s is close to 128 and σ_s is close to 64, it represents the case of the best quality image *i.e.* quality value Q is expected to be close to 1.

The four cases described above can be easily visualized from image shown in Figure 10. It shows the relationship of computed mean and standard deviation of spread with the obtained quality. X-axis in the image represents mean of the spread (μ_s), Y-axis represents standard deviation of the spread (σ_s) and a pixel intensity represents the quality value (between 0 and 1) obtained for a particular mean and standard deviation combination. Intensity values vary in the range of 0 to 1, where 0 represents the darkest pixel and 1 represents the brightest pixel. As we know for the Cases 1, 2, 3, quality is 0 and hence we can see darkest pixels in the image of Figure 10 for these cases. For Case 4 where μ_s is equal to 128 and σ_s is equal to 64, we get the brightest spot in the image representing the best quality.

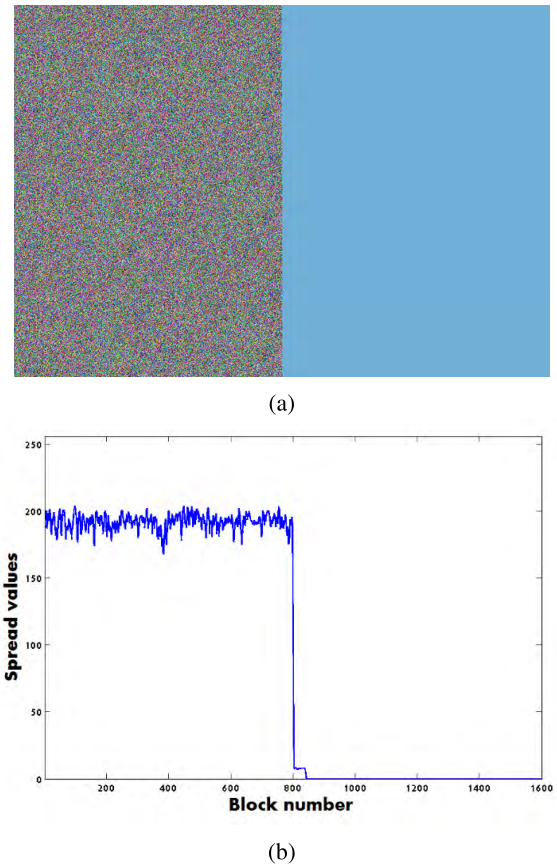

FIGURE 9. Example of an image with spread of very high standard deviation (σ_s): (a) Synthetic poor quality image with half noise and half blur, (b) spread plot of the image shown in (a) representing high standard deviation of the spread ($\sigma_s = 101$). (a) poor quality image. (b) spread corresponding to (a).

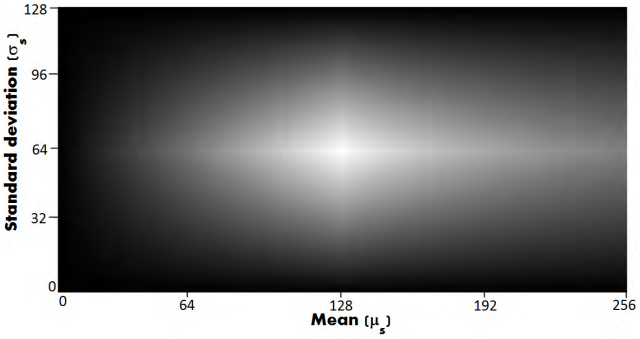

FIGURE 10. Relationship between mean μ_s, standard deviation σ_s and estimated quality. Each gray value in the image shows quality score where higher gray value shows better quality.

With the help of image presented in Figure 10, we can understand some characteristics of the relationship of μ_s, σ_s and image quality with respect to the proposed technique. We observe that in the proposed technique, values of μ_s and σ_s range between 0 to 256 and between 0 to 128 respectively. However, there may be some combinations of μ_s and σ_s which may not exist in reality. That means, there may be some intensity values (quality values) shown in the image

which may not exist in reality. For example, in the proposed technique when μ_s is equal to 256, σ_s must be only equal to 0, however image presented in Figure 10 shows quality values (which do not exist in reality) for different σ_s (from 0 to 128) for μ_s equals to 256. Another such example which we can see is when μ_s is equal to 0 and σ_s is also expected to be 0 for this (*i.e.* σ_s should be 0 when μ_s is equal to 0). However, different quality values (which again do not exist in reality) have been shown for different σ_s (0 to 128) for μ_s equals to 0 in the image.

V. EXPERIMENTAL RESULTS

A. DATABASES

The proposed technique is experimented on LIVE [34] [35] and CSIQ [36] databases. We have considered images distorted by Gaussian blur and white noise from the databases. Both these databases provide subjective quality scores in terms of realigned Different Mean Opinion Score (DMOS) [37] where the value of DMOS for each image is generated through rating given by human observers. Description of all databases is summarized in Table 1. It provides number of images in each database.

TABLE 1. Description of databases for white noise and blur.

Database	Number of images
LIVE [34]	174
CSIQ [36]	150

B. DISCUSSION ON PARAMETERS

We have observed the influence of different parameters on the proposed technique. Image block size is one of the parameters used in proposed technique. Table 2 shows top 6 experimentation results of the proposed technique using SROCC values (discussed in Section V-C) for various block sizes on LIVE database. Table 2 elucidates that the result changes when the block size is varied. This elucidates that the selection of optimum value of this parameter plays a significant role in the estimation of quality of an image in the proposed technique. In order to compute the optimal value of image block size, we experiment on randomly selected 40 images of the LIVE database. We use the obtained results of this experiment for deciding the optimum value of the block size. Table 3 presents experimental results obtained on selected 40 images. Table shows that the best performance of the proposed technique is achieved for these images when the block size is set to 50×50. Since the images used in this experiment are chosen randomly and both the databases (LIVE and CSIQ) have similar type of images, the randomly selected 40 images are believed to be the representative of both the databases. Hence we use the value of the block size obtained in this experiment while experimenting with both databases.

Another parameter used in the proposed technique is α which is used in Equation 1 to compute the spread of a distribution. Instead of considering just one value of α for spread computation, we consider a set of values of α in the range of 0.001 to 0.1 with an interval of 0.05 and compute spread for each value. Further, we take the average of the spread values obtained for various values of α to decide the final spread of a distribution. We also investigate the influence of selection of different mother wavelets (*viz.* Morlet, Cauchy and Paul) on the proposed technique. Table 4 shows results of the proposed technique using different mother wavelets on randomly selected 40 images and it is seen that the proposed technique performs the best when Mexican hat mother wavelet is used. We use the same mother wavelet for performing experiment on the complete database.

C. QUANTITATIVE EVALUATION

DMOS (given by the databases) has been used to assess the performance of the proposed technique. We have followed the performance evaluation procedure given by the Video Quality Expert Group (VQEG) [37] for the evaluation of the proposed technique. Spearman rank-order correlation coefficient (SROCC) and root mean square error (RMSE) are used as evaluation metrics in the proposed technique. RMSE computes error between objective score and DMOS. Lower value of RMSE shows better results. SROCC is considered the most popular and reliable evaluation metric which provides prediction monotonicity. The absolute higher value of SROCC shows better results. In our study, we use both SROCC and RMSE for comparing the techniques; however, rely more on SROCC. For example, we set the parameters of the proposed technique by making use of SROCC value.

RMSE and SROCC make use of subjective (Q_s) and objective (Q_o) quality scores in their computation. SROCC is computed directly by using the subjective (Q_s) and objective (Q_o) quality score; however, to compute RMSE, VQEG suggest the use of non-linear mapping between quality scores obtained by the proposed technique and DMOS values. Non-linear mapping is performed using a logistic function [37].

The scatter plots of quality obtained by the proposed technique versus DMOS on LIVE database are shown in Figure 11. It is clear from the plots that the correlation values (SROCC) are high for both white noise as well as for Gaussian blur which shows that quality scores computed by the proposed technique matches well with DMOS (subjective quality scores).

D. PERFORMANCE COMPARISON

The proposed technique has been compared with several existing NR-IQA techniques such as NIQE [26], LQF [24], QAC [23], NRQI [25], BIQES [27], SA-SS, SA-ZC [28] and NOMDA [29]. Techniques [26], [24], [23] and [25] have utilized training without subjective scores (DMOS) while techniques presented in [28]–[29] do not require training.

Results of various techniques (except BIQES and NOMDA) reported in the tables (Tables 5 to 10) for comparison have been taken from the respective papers. For BIQES and NOMDA technique, we have made use of available code

TABLE 2. Results of the proposed technique for different block size on entire LIVE database.

Block size	SROCC value: Gaussian blur	SROCC value: white noise
20×20	0.8103	0.9421
25×25	0.8491	0.9511
40×40	0.8617	0.9630
50×50	**0.9169**	**0.9697**
100×100	0.9010	0.9640
200×200	0.8803	0.9132

TABLE 3. Results of the proposed technique for different block size on 40 randomly selected images from LIVE database.

Block size	SROCC value: Gaussian blur	SROCC value: white noise
20×20	0.5229	0.5576
25×25	0.6985	0.7149
40×40	0.8356	0.9145
50×50	**0.8865**	**0.9587**
100×100	0.7124	0.7369
200×200	0.6527	0.6621

TABLE 4. Results of the proposed technique using different wavelets on LIVE database.

Wavelet	SROCC value: Gaussian blur	SROCC value: white noise
Paul	0.3637	0.9031
Cauchy	0.4104	0.7261
Morlet	0.2812	0.8818
Mexican hat	**0.9169**	**0.9697**

TABLE 5. Result comparison with training based techniques for white noise on LIVE database.

Quality measure	Type	Training	RMSE[1]	SROCC[2]
QAC[23]	NR	Yes	-	0.9613
LQF[24]	NR	Yes	-	0.77
NRQI[25]	NR	Yes	-	0.9357
NIQE[26]	NR	Yes	-	0.9662
Proposed technique	NR	No	**6.5**	**0.9697**

1. RMSE is the error and its lower is better.

2. SROCC is correlation and its absolute higher value is better.

- indicates that authors have not reported results.

to generate results in required form. For NOMDA technique, the results reported in this paper are based on considering 40 images for setting of parameters.

Tables 5 and 6 show comparison between the proposed technique and techniques which use training for estimation of white noise and Gaussian blur respectively on LIVE database. Tables 7 and 8 show the comparative results of the proposed technique with IQA techniques which do not use training for white noise and Gaussian blur respectively on LIVE database. Comparative results on CSIQ database are shown in Table 9, Table 10, Table 11 and Table 12. Tables 9 and 10 show comparison between the proposed technique and techniques which use training for white noise and Gaussian blur respectively. Tables 11 and 12 show the comparative results of the proposed technique with IQA techniques which do not use training for white noise and Gaussian blur respectively.

From the comparisons presented in Tables, 5, 6, 7, 8, 9, 10, 11 and 12 we make following observations.

1) Table 5 presents comparative results of the proposed technique with well known training based IQA techniques for images affected by white noise on LIVE database. We see that the proposed technique is superior to all the techniques which use training (*viz.* QAC, LQF, NRQI and NIQE).
2) Table 6 presents comparative results of the proposed technique with IQA techniques which use training for

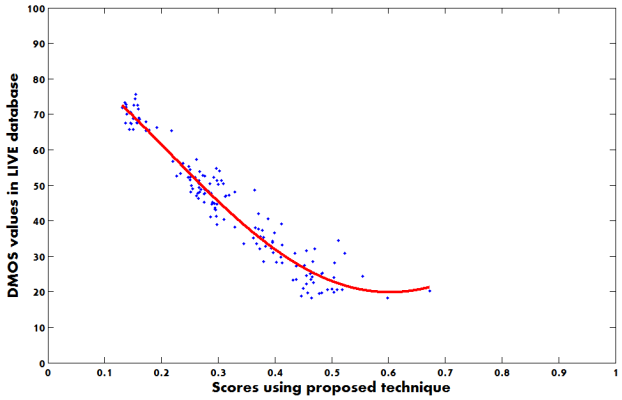

(a) SROCC: 0.9697

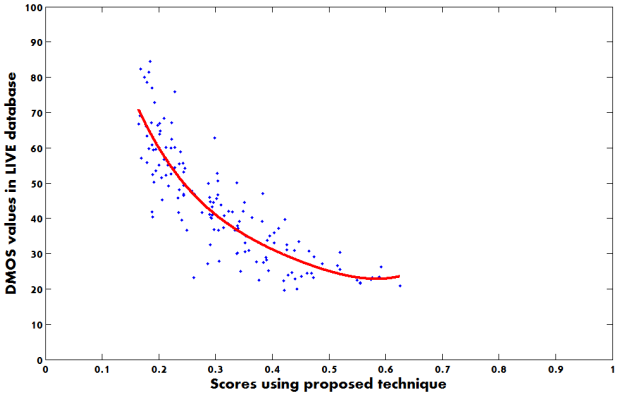

(b) SROCC: 0.9169

FIGURE 11. Scatter plots of DMOS versus quality scores computed using the proposed technique: (a) plot for white noise distortion (b) plot for Gaussian blur distortion.

TABLE 6. Result comparison with training based techniques for Gaussian blur on LIVE database.

Quality measure	Type	Training	RMSE	SROCC
QAC[23]	NR	Yes	-	0.9094
LQF[24]	NR	Yes	-	0.86
NRQI[25]	NR	Yes	-	0.8562
NIQE[26]	NR	Yes	-	0.9341
Proposed technique	NR	No	**7.865**	**0.9169**

Gaussian blur images on LIVE database. The proposed technique clearly outperforms QAC, LQF and NRQI techniques. In this case, only NIQE technique has shown little better performance as compared to the proposed technique; however, NIQE is a training based IQA technique and the proposed technique is free from any training.

3) Table 7 shows comparison between the proposed technique and no-reference based IQA techniques which do not use training for white noise on LIVE database. We see that the proposed technique clearly outperforms SS-ZC, SA-SS and BIQES presented in the table. The proposed technique produces comparable results to NOMDA technique (particularly in terms of SROCC).

TABLE 7. Result comparison with no-training based techniques for white noise on LIVE database.

Quality measure	Type	Training	RMSE	SROCC
SA-SS[28]	NR	No	6.839	0.959
SA-ZC[28]	NR	No	8.717	0.931
BIQES[27]	NR	No	7.713	0.9694
NOMDA[29]	NR	No	6.139	0.9741
Proposed technique	NR	No	**6.5**	**0.9697**

TABLE 8. Result comparison with no-training based techniques for Gaussian blur on LIVE database.

Quality measure	Type	Training	RMSE	SROCC
SA-SS[28]	NR	No	7.876	0.888
SA-ZC[28]	NR	No	7.920	0.892
BIQES[27]	NR	No	8.12	0.9071
NOMDA[29]	NR	No	9.313	0.9015
Proposed technique	NR	No	**7.865**	**0.9169**

TABLE 9. Result comparison with training based techniques for white noise on CSIQ database.

Quality measure	Type	Training	RMSE	SROCC
QAC[23]	NR	Yes	-	0.8222
NRQI[25]	NR	Yes	-	0.8034
NIQE[26]	NR	Yes	-	0.8098
Proposed technique	NR	No	**0.0931**	**0.8935**

TABLE 10. Result comparison with training based techniques for Gaussian blur on CSIQ database.

Quality measure	Type	Training	RMSE	SROCC
QAC[23]	NR	Yes	-	0.8363
NRQI[25]	NR	Yes	-	0.8743
NIQE[26]	NR	Yes	-	0.8953
Proposed technique	NR	No	**0.1626**	**0.8010**

4) From Table 8, we observe that the proposed technique also outperforms all no-reference, no-training based techniques (*viz.*SS-ZC, SA-SS, BIQES and NOMDA) for Gaussian blur distortion on LIVE database.
5) Table 9 presents that the proposed technique is superior to no-reference, training based techniques such as QAC, NRQI and NIQE for white noise distortion on CSIQ database.
6) From the Table 10, we can see that the proposed technique gives satisfactory performance as compared to no-reference, training based techniques such as QAC, NRQI and NIQE for Gaussian blur on CSIQ database. However, it is noted that QAC, NRQI and NIQE techniques use training and the proposed technique is free from any training.
7) Table 11 presents comparison between the proposed technique and no-reference no-training based techniques BIQES and NOMDA for white noise on CSIQ database. We observe that the proposed technique is superior to BIQES for both SROCC and RMSE metrics. The proposed technique results are comparable to NOMDA technique in case of white noise.

TABLE 11. Result comparison with no-training based techniques for white noise on CSIQ database.

Quality measure	Type	Training	RMSE	SROCC
BIQES[27]	NR	No	0.0947	0.8234
NOMDA[29]	NR	No	0.0823	0.8953
Proposed technique	NR	No	**0.0931**	**0.8935**

TABLE 12. Result comparison with no-training based techniques for Gaussian blur on CSIQ database.

Quality measure	Type	Training	RMSE	SROCC
BIQES[27]	NR	No	0.1611	0.8218
NOMDA[29]	NR	No	0.1653	0.8001
Proposed technique	NR	No	**0.1626**	**0.8010**

TABLE 13. Comparison of quality estimation time per image (in seconds) for the proposed and the NOMDA techniques.

Technique	Execution time
NOMDA [29]	4.10
Proposed technique	1.91

8) From Table 12, we observe that the proposed technique outperforms NOMDA technique for both SROCC and RMSE metrics for Gaussian blur on CSIQ database. The proposed technique gives a comparable performance as compared to no-reference, no-training based BIQES technique. Though BIQES is a no-reference, no-training based technique like the proposed technique, it selects customized value of the parameter used to compute contrast sensitivity function for different databases. In the proposed technique, we have experimented on different databases keeping values of all the parameters same.

Based on our experimental analysis conducted over LIVE and CSIQ databases, we conclude that the proposed technique performs very well and gives good results. In spite of the proposed technique being a no-reference, no-training based technique, it produces encouraging results as compared to no-reference, training based techniques such as QAC, LQF, NRQI and NIQE and no-reference, no-training based techniques such as NOMDA, BIQES, SS-ZC and SA-SS.

Particularly, when we compare the results of the proposed technique with our earlier proposed technique (NOMDA), we observe that the performance of the proposed technique is mostly superior or comparable with NOMDA technique. Moreover, in terms of execution time, the proposed technique performs much superior to NOMDA technique. Comparison of execution time of the proposed technique and NOMDA technique is presented in Table 13. It can be clearly seen that the time required for the quality estimation by the proposed technique is almost half of that required by NOMDA technique.

VI. CONCLUSION

This paper has proposed a no-reference no-training based IQA technique using CWT. The proposed technique has used CWT to analyze the presence of the disturbances affecting the naturalness of the image to assess its quality. The technique has taken into account two distortions namely, white noise and Gaussian blur in quality estimation and does not require any training. Experimental analysis has shown that the quality values estimated by the proposed technique for different images of the databases are very similar to that of human subjective opinions. It is also seen that the performance of the proposed technique is superior as compared to well known no-reference, no-training based IQA techniques.

REFERENCES

[1] W. Lin and C.-C. Jay Kuo, "Perceptual visual quality metrics: A survey," *J. Vis. Commun. Image Represent.*, vol. 22, no. 4, pp. 297–312, 2011.

[2] X. Gao, W. Lu, D. Tao, and X. Li, "Image quality assessment and human visual system," *Proc. SPIE*, vol. 7744, p. 77440Z, Aug. 2010.

[3] H. R. Wu and K. R. Rao, *Digital Video Image Quality and Perceptual Coding*. Boca Raton, FL, USA: CRC Press, 2005.

[4] Z. P. Sazzad, Y. Kawayoke, and Y. Horita, "No reference image quality assessment for JPEG2000 based on spatial features," *Signal Process., Image Commun.*, vol. 23, no. 4, pp. 257–268, 2008.

[5] Z. Wang, A. C. Bovik, and B. L. Evan, "Blind measurement of blocking artifacts in images," in *Proc. IEEE Int. Conf. Image Process. (ICIP)*, vol. 3, Sep. 2000, pp. 981–984.

[6] A. C. Bovik and S. Liu, "DCT-domain blind measurement of blocking artifacts in DCT-coded images," in *Proc. IEEE Int. Conf. Acoust., Speech, Signal Process. (ICASSP)*, vol. 3, May 2001, pp. 1725–1728.

[7] H. R. Wu and M. Yuen, "A generalized block-edge impairment metric for video coding," *IEEE Signal Process. Lett.*, vol. 4, no. 11, pp. 317–320, Nov. 1997.

[8] L. Li, W. Lin, and H. Zhu, "Learning structural regularity for evaluating blocking artifacts in JPEG images," *IEEE Signal Process. Lett.*, vol. 21, no. 8, pp. 918–922, Aug. 2014.

[9] P. Marziliano, F. Dufaux, S. Winkler, and T. Ebrahimi, "Perceptual blur and ringing metrics: Application to JPEG2000," *Signal Process., Image Commun.*, vol. 19, no. 2, pp. 163–172, Feb. 2004.

[10] L. Liang, S. Wang, J. Chen, S. Ma, D. Zhao, and W. Gao, "No-reference perceptual image quality metric using gradient profiles for JPEG2000," *Signal Process., Image Commun.*, vol. 25, no. 7, pp. 502–516, Aug. 2010.

[11] E. Ong *et al.*, "A no-reference quality metric for measuring image blur," in *Proc. 7th Int. Symp. Signal Process. Appl.*, vol. 1, Jul. 2003, pp. 469–472.

[12] L. Li, W. Lin, X. Wang, G. Yang, K. Bahrami, and A. C. Kot, "No-reference image blur assessment based on discrete orthogonal moments," *IEEE Trans. Cybern.*, vol. 46, no. 1, pp. 39–50, Jan. 2016.

[13] M.-J. Chen and A. C. Bovik, "No-reference image blur assessment using multiscale gradient," *EURASIP J. Image Video Process.*, vol. 2011, no. 1, pp. 1–11, 2011.

[14] L. Li, W. Xia, W. Lin, Y. Fang, and S. Wang, "No-reference and robust image sharpness evaluation based on multiscale spatial and spectral features," *IEEE Trans. Multimedia*, vol. 19, no. 5, pp. 1030–1040, May 2017.

[15] P. Joshi, S. Prakash, and S. Rawat, "Continuous wavelet transform-based no-reference quality assessment of deblocked images," *Vis. Comput.*, pp. 1–10, Nov. 2017. [Online]. Available: https://doi.org/10.1007/s00371-017-1460-z

[16] A. K. Moorthy and A. C. Bovik, "A two-step framework for constructing blind image quality indices," *IEEE Signal Process. Lett.*, vol. 17, no. 5, pp. 513–516, May 2010.

[17] M. A. Saad, A. C. Bovik, and C. Charrier, "Blind image quality assessment: A natural scene statistics approach in the DCT domain," *IEEE Trans. Image Process.*, vol. 21, no. 8, pp. 3339–3352, Aug. 2012.

[18] A. K. Moorthy and A. C. Bovik, "Blind image quality assessment: From natural scene statistics to perceptual quality," *IEEE Trans. Image Process.*, vol. 20, no. 12, pp. 3350–3364, Dec. 2011.

[19] L. Liu, H. Dong, H. Huang, and A. C. Bovik, "No-reference image quality assessment in curvelet domain," *Signal Process. Image Commun.*, vol. 29, no. 4, pp. 494–505, Apr. 2014.
[20] A. Mittal, A. K. Moorthy, and A. C. Bovik, "No-reference image quality assessment in the spatial domain," *IEEE Trans. Image Process.*, vol. 21, no. 12, pp. 4695–4708, Dec. 2012.
[21] H. Tang, N. Joshi, and A. Kapoor, "Learning a blind measure of perceptual image quality," in *Proc. IEEE Conf. Comput. Vis. Pattern Recognit. (CVPR)*, Jun. 2011, pp. 305–312.
[22] P. Ye and D. Doermann, "No-reference image quality assessment using visual codebooks," *IEEE Trans. Image Process.*, vol. 21, no. 7, pp. 3129–3138, Jul. 2012.
[23] W. Xue, L. Zhang, and X. Mou, "Learning without human scores for blind image quality assessment," in *Proc. IEEE Conf. Comput. Vis. Pattern Recognit. (CVPR)*, Jun. 2013, pp. 995–1002.
[24] A. Mittal, G. S. Muralidhar, J. Ghosh, and A. C. Bovik, "Blind image quality assessment without human training using latent quality factors," *IEEE Signal Process. Lett.*, vol. 19, no. 2, pp. 75–78, Feb. 2012.
[25] C. Li, Y. Ju, A. C. Bovik, X. Wu, and Q. Sang, "No-training, no-reference image quality index using perceptual features," *Opt. Eng.*, vol. 52, no. 5, p. 057003, 2013.
[26] A. Mittal, R. Soundararajan, and A. C. Bovik, "Making a 'completely blind' image quality analyzer," *IEEE Signal Process. Lett.*, vol. 20, no. 3, pp. 209–212, Mar. 2013.
[27] A. Saha and Q. M. J. Wu, "Utilizing image scales towards totally training free blind image quality assessment," *IEEE Trans. Image Process.*, vol. 24, no. 6, pp. 1879–1892, Jun. 2015.
[28] J. Zhang, T. M. Le, S. H. Ong, and T. Q. Nguyen, "No-reference image quality assessment using structural activity," *Signal Process.*, vol. 91, no. 11, pp. 2575–2588, 2011.
[29] P. Joshi and S. Prakash, "Retina inspired no-reference image quality assessment for blur and noise," *Multimedia Tools Appl.*, vol. 76, no. 18, pp. 18871–18890, 2017.
[30] E. H. Land and J. J. McCann, "Lightness and Retinex theory," *J. Opt. Soc. Amer.*, vol. 61, no. 1, pp. 1–11, 1971.
[31] S. Wang, J. Zheng, H.-M. Hu, and B. Li, "Naturalness preserved enhancement algorithm for non-uniform illumination images," *IEEE Trans. Image Process.*, vol. 22, no. 9, pp. 3538–3548, Sep. 2013.
[32] A. Grossmann and J. Morlet, "Decomposition of hardy functions into square integrable wavelets of constant shape," *SIAM J. Math. Anal.*, vol. 15, no. 4, pp. 723–736, 1984.
[33] D. L. Fugal, *Conceptual Wavelets in Digital Signal Processing*. San Diego, CA, USA: Space and Signals Technical Publishing, 2009.
[34] L. Cormack, H. R. Sheikh, Z. Wang, and A. C. Bovik, "LIVE image quality assessment database release 2," Univ. Texas Austin, Austin, TX, USA, Tech. Rep., 2006. [Online]. Available: http://live.ece.utexas.edu/research/quality
[35] H. R. Sheikh, M. F. Sabir, and A. C. Bovik, "A statistical evaluation of recent full reference image quality assessment algorithms," *IEEE Trans. Image Process.*, vol. 15, no. 11, pp. 3440–3451, Nov. 2006.
[36] E. C. Larson and D. M. Chandler, "Most apparent distortion: Full-reference image quality assessment and the role of strategy," *J. Electron. Imag.*, vol. 19, no. 1, p. 011006, 2010.
[37] VQEG. (2009). *Final Report From the Video Quality Experts Group on the Validation of Reduced-Reference and no-Reference Objective Models for Standard Definition Television, Phase-I*. [Online]. Available: http://www.vqeg.org/s

PIYUSH JOSHI received the B.E. degree in computer science and engineering form Rajiv Gandhi Proudyogiki Vishwavidyalaya, Bhopal, India, and the M.Tech. degree in information technology from the Indian Institute of Information Technology at Allahabad, Allahabad. He is currently a Ph.D. Scholar with the Department of Computer Science and Engineering, IIT Indore, India. His research interests include image processing and pattern recognition.

SURYA PRAKASH received the M.S. degree in computer science and engineering from IIT Madras, India, and the Ph.D. degree in computer science and engineering from IIT Kanpur, India. He is currently an Assistant Professor with the Department of Computer Science and Engineering, IIT Indore, India. He has published several research articles in peer-reviewed international journals and conferences. He has also co-authored two books *IT Infrastructure and Its Management* (India: Tata McGraw-Hill) and *Ear Biometrics in 2D and 3D: Localization and Recognition* (Springer). His research interests include image processing, computer vision, pattern recognition, biometrics, and identity and infrastructure management. He has also been in the program committees of several international conferences in the field of pattern recognition, image processing, and intelligent computing.